






# Role of Seismic Refraction Tomography (SRT) in bedrock mapping; case study from industrial zone, Ain-Sokhna area, Egypt

Muhammad A. EL HAMEEDY<sup>1,\*</sup> , Walid M. MABROUK<sup>1</sup> ,  
Said DAHROUG<sup>1</sup> , Mohamed S. YOUSSEF<sup>2</sup> ,  
Ahmed M. METWALLY<sup>1</sup> 

<sup>1</sup> Department of Geophysics, Faculty of Science, Cairo University, Egypt

<sup>2</sup> Nuclear Materials Authority, Exploration Division, Maadi, Cairo, Egypt

**Abstract:** In this study, eighteen compressional P-wave seismic refraction profiles survey was conducted on the western side of the Gulf of Suez, Egypt, to map bedrock topography, which is vital information in foundation pole placement and design for large factory construction. The configuration of the seismic survey consists of 10 metres geophone intervals (12 and 24 channels) with a total survey length of 3150 metres survey length. The seismic compressional wave velocity distribution reveals three layers ranging from (400 to 1100 m/s), (1200 to 2000 m/s), and (2200 to 3500 m/s). According to the data, the first low-velocity layer represents unconsolidated Wadi sediments. The second layer, on the other hand, comprises consolidated Wadi sediments, while the third layer comprises fractured to intact sandstone bedrock. The thickness of the first layer is believed to be between 0.5 and 10 m, while the thickness of the second layer is between 8.5 and 25 m. Pseudo-3D model of velocity distribution was constructed, revealing the presence of several low-velocity zones at a depth ranging from 15 to 32 m. Then, the topography of the non-rippable sandstone rock mass was mapped utilizing 3-D model. Finally, the correlation between seismic refraction tomography (SRT) results and nearby well logging dataset drilled by the Egyptian Geological Survey and Mining Authority (EGSMA) matched quite well. It may be inferred that, up to a depth of 15 to 32 metres, there is a high-velocity rock layer suitable for constructing deep foundations for multiple levels of the mega factory.

**Key words:** seismic refraction tomography, tomographic inversion, bedrock mapping, geotechnical geophysics, foundation poles, 3D SRT

## 1. Introduction

Poor subsurface understanding under the proposed building usually throws off the construction schedules, slows the implementation of design, and even-

\*corresponding author, e-mail: mashraf@sci.cu.edu.eg

tually impedes the project's progress. Consequently, it is essential to examine the subsurface characteristics of a given area using geophysical investigations before initiating civil construction. Trenching and boreholes are often used in conventional geotechnical studies to gather scattered and discrete data points.

As a result, adopting the seismic refraction tomography (SRT) technique has been shown to save time and money since it is a non-destructive technique that provides information on the subsurface rock mass characteristics from site investigations to continental studies (*Schlundwein et al., 2003*), allowing for the efficient and effective selection of various geotechnical studies. As both of them must be effectively combined, first to support SRT findings, and secondly, as SRT results recommend where to do such geotechnical tests, SRT may thus be a way to overcome these limits without ignoring geotechnical investigations.

Traditional delay time or generalised reciprocal method (GRM) refraction research efforts simplify velocity structure assumptions where the subsurface is depicted as a layered medium with specific seismic velocities in each layer. Each ground layer's thickness and dip angle are calculated using this assumption based on the travel time of the refracted seismic waves (*Sheriff and Geldart, 1995*). Unfortunately, that contradicts frequently observed near-surface characteristics like heterogeneity, lateral discontinuities, and gradients (*Sheehan et al., 2005*).

Nevertheless, refraction tomography is not subject to these constraints (*Thurber and Ritsema, 2007; Whiteley et al., 2020*). Therefore, it is able to resolve velocity gradients and lateral velocity changes and can be applied in geological conditions where conventional refraction techniques fail, such as areas of compaction, karst, and fault zones (*Hiltunen and Cramer, 2008; Metwally et al., 2017; Brixová et al., 2018; Akingboye and Ogunyele, 2019; Herlambang and Riyanto, 2021*). Several studies (*White, 1989; Nurhandoko et al., 1999; Leucci et al., 2007; Azwin et al., 2013; Bery, 2013*) prove the high applicability of the SRT technique in subsurface velocity modelling and ground exploration. They showed that seismic refraction tomography performed well in many situations where traditional refraction techniques failed to identify vertical and horizontal velocity gradients. Utilization of seismic refraction in geotechnical investigations studies related to foundation evaluation problems is widely adopted (*Oyedele et al., 2011; Ozcep and Ozcep,*

2011; Jamiolkowski, 2012; Butchibabu et al., 2019a,b; Butchibabu et al., 2023) primarily to assess the substratum conditions at strategic locations.

In our case, a major industrial zone is under construction on the western side of the Gulf of Suez (GOS) near the new Suez port. The need to understand the topography of the bedrock is critical for foundation pole design and placement, as well as to classify the layers of the subsurface with the aid of the nearby wireline logging dataset of Suez well-3, drilled by the Egyptian Geological Survey and Mining Authority (EGSMA) which provides geological data as a reference point for this research seismic refraction method.

Several geophysical studies investigated the Ain-Sokhna area (*El-Behiry et al., 2006; Attwa and Henaish, 2018; Younis et al., 2019; Youssef, 2020; Araffa et al., 2022*) focusing on groundwater exploration. *Othman et al. (2015)* conducted a seismic refraction survey near the study area, utilizing the generalized reciprocal method (GRM) in the interpretation. Finally, *Mekkawi et al. (2022)* studied the potential of geothermal resources in the area utilizing magnetotelluric and magnetic methods.

The current research discusses seismic refraction investigations, consisting of 18 profiles with a total length of approximately 3150 m, along Cairo-Suez Road at the Ain-Sokhna area, where bedrock depth and topography were investigated. 2D seismic tomograms were interpreted, and 3D models were generated to map the lateral distribution of the layers' depths.

## 2. Geographical location and geology of the area

The Suez Governorate's Ain-Sokhna area is located on Egypt's western shore of the Gulf of Suez (Fig. 1). According to geomorphology, the Ain-Sokhna region is broken down into four primary units:

- **Coastal plain unit:** This low geographical area is between the Gulf of Suez to the east and the steep and hilly terrain to the west. It is primarily covered with Quaternary clastic deposits, as well as thick, widespread gravelly and sandy layers, forming a plain that gradually dips towards the sea.
- **Highlands:** The peaks of the northern Galala and Gabal Ataqa represent this highland region. High vertical scarps are produced by the imposing

mountainous rock known as Gabal Ataqa. On their northern and eastern slopes, the highest point is 900 metres or thereabouts above sea level. The Northern Galala is a significant area in the northern part of the Gulf of Suez.

- **Low-lying hill unit:** Most of their surface is made up of rocks from the Upper Eocene to Miocene.
- **Drainage pattern:** There are four important drainage basins in the Ain Al-Sokhna area. From north to south, the basins mentioned above are the Wadi Hagoul basin, the South Wadi Hagoul basin, the Wadi Akheider Bada basin, and the Wadi Ghwieba basin.

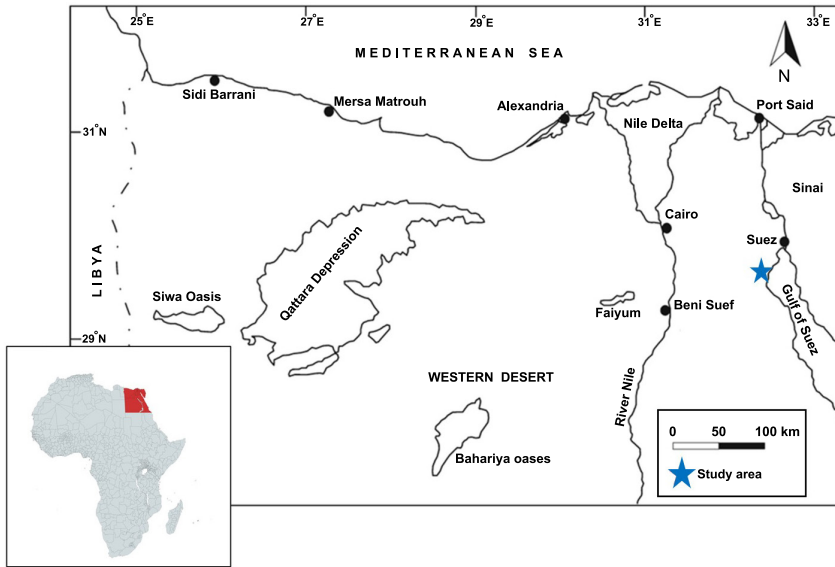


Fig. 1. Location map of the study area.

The rock units identified within the study area are shown in Fig. 2. *Abu El-Enain et al. (1997)* separated the Eocene rocks into the Middle Eocene (Mokattam Formation) and Upper Eocene (Maadi Formation). The Oligocene rocks lie unconformably on top of the Upper Eocene clastics. Upper Eocene clastic rocks are composed of volcanic (basaltic sheets and doleritic intrusions) and sedimentary (sandstone, quartzite, and flint gravel),

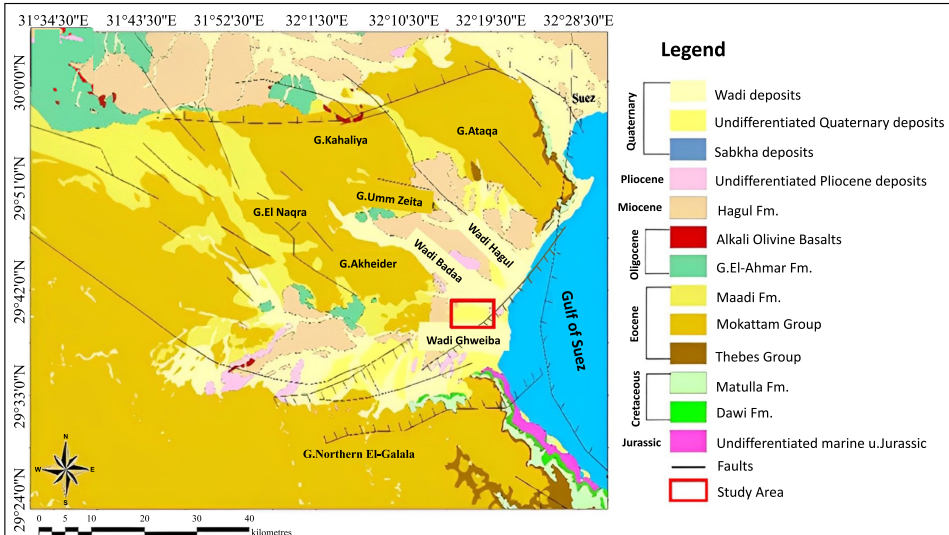


Fig. 2. Geological map of the western side of Gulf of Suez after (Conco, 1987).

which are Oligocene rock types. The Hagul Formation (Upper Miocene) and Sadat Formation (Lower Miocene), in that order, are representative of Miocene rocks. The majority of the Pliocene deposits are composed of different gravels and flint pebbles in sand, while in certain areas, these gravels also include limestone and flint pebbles (Salem, 1988). Two types of Quaternary sediments (Holocene and Pleistocene) are composed of gravels, cobbles, boulders, and sands and may be found as Quaternary terraces and alluvial deposits (Reynolds, 1979).

According to Youssef and Abdel-Rahman (1978), the study area and the nearby areas are part of a massive graben where multiple gently sloping fault blocks protrude above the surface. To ascertain the deformation style that affects the area and the anticipated stress direction, Salem (1988) assessed the structural components of the study area and its surroundings. He also discovered a connection between the two provinces (the Gulf of Suez to the east and the Cairo-Suez region to the north) and their deformation styles. He observed that most of these faults are normal, and just a small number of them are diagonal, with substantial dip-slip movement and negligible strike-slip components.

*Sultan et al. (2017)* classified the major fault trends into NNW–SSE, E–W, and WNW–ESE faults. The bulk of the faults are located in a north-west–southeast direction. They influence the Eocene limestone plateau and delimit the main Wadis of the area under investigation, such as Wadi Hagul, Wadi Badaa, and Wadi Ghweiba. The second-most significant faults are the east-west faults. It is thought to have begun in the late Eocene and continued into the Oligocene (*Salem, 1988*). Finally, the WNW–ESE faults are distributed throughout the low, hilly terrain in the depression between Gebel Northern El-Galala and Gebel Ataqa (*Moustafa and Khalil, 2020*).

### 3. Data acquisition and methodology

Seismic energy is incorporated in the seismic refraction technique, and it returns to the surface after travelling through the subsurface through refracted ray routes. A direct or refracted ray is always indicated by the first seismic waves that arrive at a detector (geophone) far from a seismic source (*Reynolds, 1997*). The P-wave velocity increases as a result of the confining pressure (*Han et al., 1986*). Due to progressive consolidation and cementation, the shale and sandstone velocities consistently rise with burial depth and age (*Avseth et al., 2001*). The rippability chart (Fig. 3) displays a material’s potential for excavation by Caterpillar’s D8R/D8T ripper in accordance with its seismic P-wave velocity.

Eighteen seismic profiles were obtained in the study area. The 240-metres-long extension of the profiles has a NE–SW trend. On the other hand, the 120-metres-long profiles were trending NW–SE, as shown in Fig. 4. A geophone interval of 10 metres and ten shot-gathers for each spread in the forward, reverse, split, and offset directions were conducted. The shallow seismic refraction field dataset was obtained using a Geometrix 24-channel seismograph model 1125E and McSEIS-SX equipped with 24 very sensitive geophones and a 15-kg sledgehammer as an energy source.

Distance between the Suez well-3 and seismic line positions is approximately 2 km. The primary result of the field work is the shot record. The direct and refracted waves that the geophones receive are the most significant initial arrivals and were used to go through the workflow as indicated in Fig. 5.

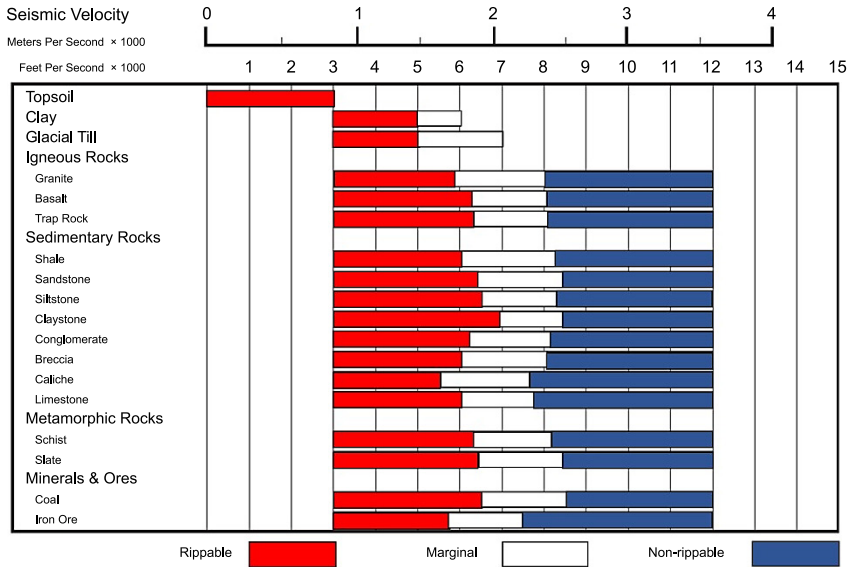


Fig. 3. Rippability chart displaying the correlation between seismic compressional-wave velocities, lithologic types, and rippability classification (Caterpillar, 2010).

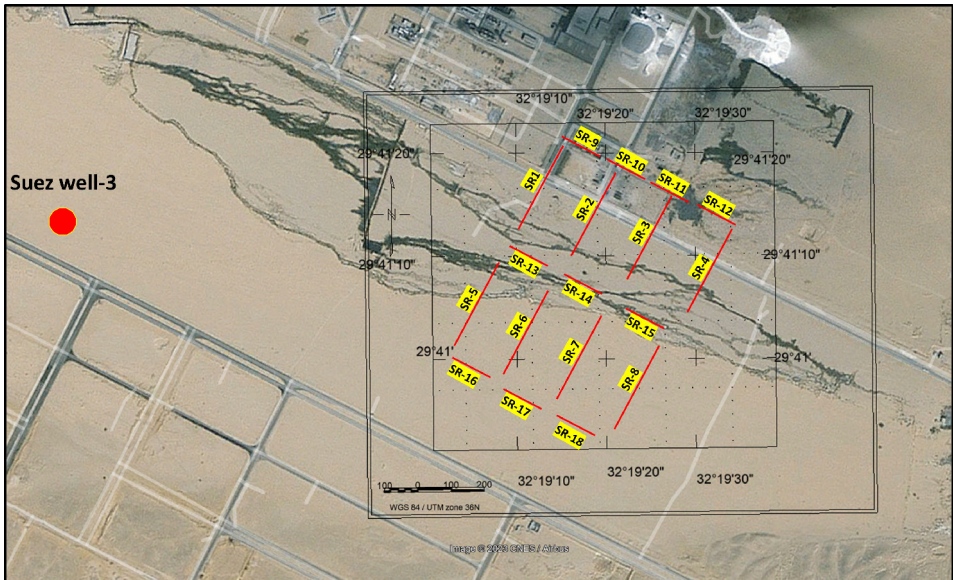


Fig. 4. Landsat imagery overlain by the survey layout and well location.

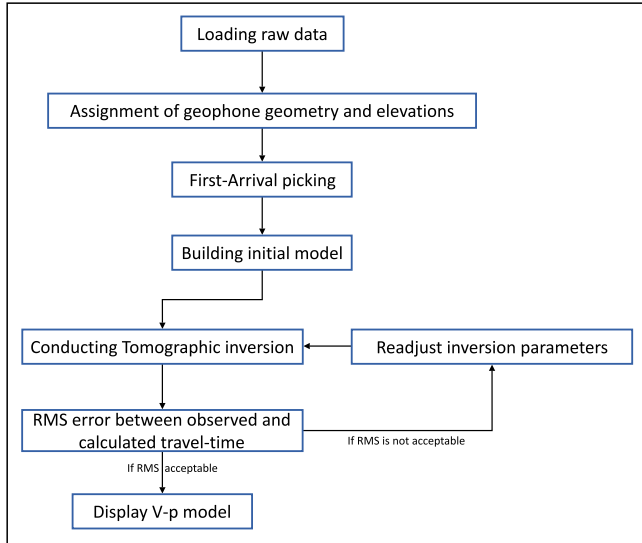


Fig. 5. Simplified flow chart for tomographic inversion process to obtain P-wave velocity model.

An initial model for the tomographic inversion was constructed using the first arrival times for the profiles. The properties of the initial velocity model have a significant impact on the final model in this type of inversion. A velocity model was created for each line after several rounds of testing and based on conventional interpretation methods, i.e., Plus-Minus (*Hagedoorn, 1959*), and GRM (*Palmer, 1981*).

#### 4. Results and discussion

The data acquired from the field records and their analysis show that the P-wave velocities are computed as follows:

- i. Unconsolidated Wadi sediments at the top with a P-wave velocity range of ( $V_{p1} = 400 - 1100$  m/s), in which the thickness of this layer ranges between 0.5 m and 10 m.
- ii. The second layer's velocity range,  $V_{p2} = 1200 - 2000$  m/s, relates to consolidated Wadi sediments, and the thickness of this layer varies between 8.5 and 25 m.



iii. The third layer is characterized by a high seismic velocity range,  $V_p3 = 2200 - 3500$  m/s, that coincides with a sandstone layer (hard to fractured sandstone).

In the area under investigation, the eighteen seismic tomograms demonstrate three main seismic strata (Figs. 6 to 8). The tomograms were used

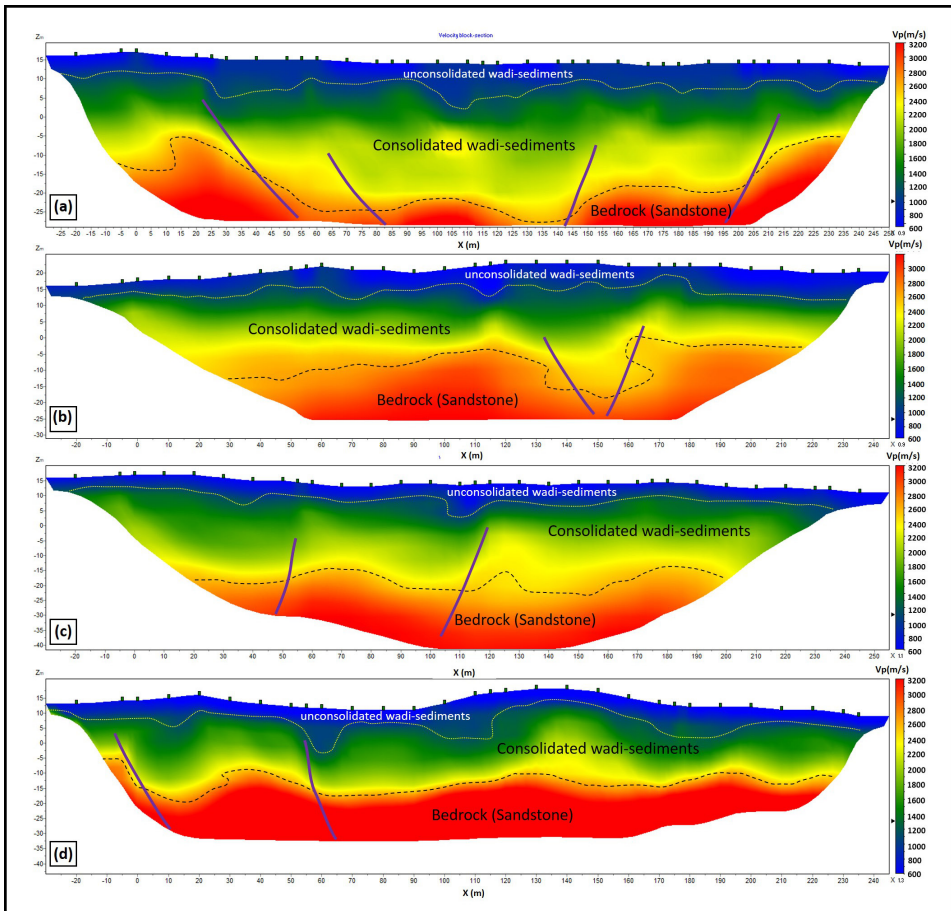


Fig. 6. Tomographic inversion results for (a) Profile SR-1; (b) Profile SR-2; (c) Profile SR-3; (d) Profile SR-4. Dashed line indicates iso-velocity of 2300 m/s which represents top non-rippable sandstone bedrock, and yellow-dotted line represents bottom boundary of Quaternary unconsolidated sandstone. Solid purple lines represent a fault structure.

to calculate the P-wave velocities, thicknesses, and depths of different rock units.

As discussed earlier in Section 2, the study area is characterized by a complex history of extensional deformation related to the opening of the Gulf of Suez and the Red Sea. The primary geological structure consists

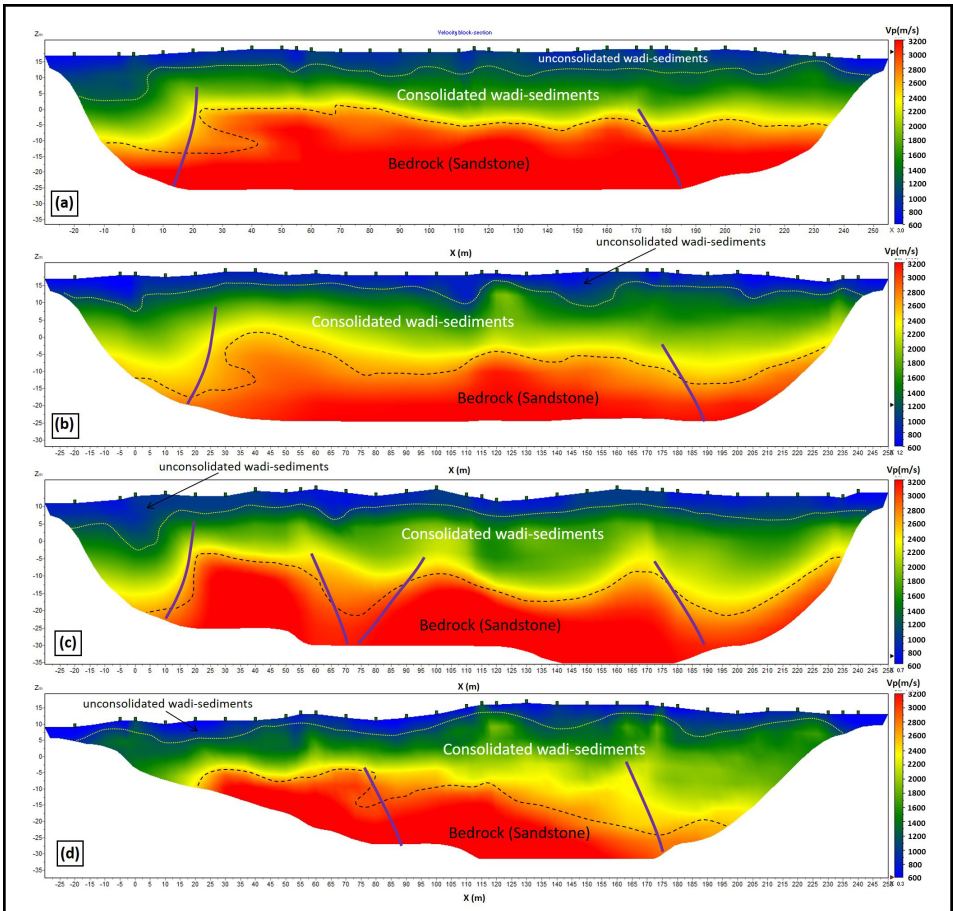


Fig. 7. Tomographic inversion results for (a) Profile SR-5; (b) Profile SR-6; (c) Profile SR-7; (d) Profile SR-8. Black-dashed line indicates iso-velocity of 2300 m/s which represents top of non-rippable sandstone bedrock, and yellow-dotted line represents bottom boundary of Quaternary unconsolidated sandstone. Solid purple lines represent a fault structure.

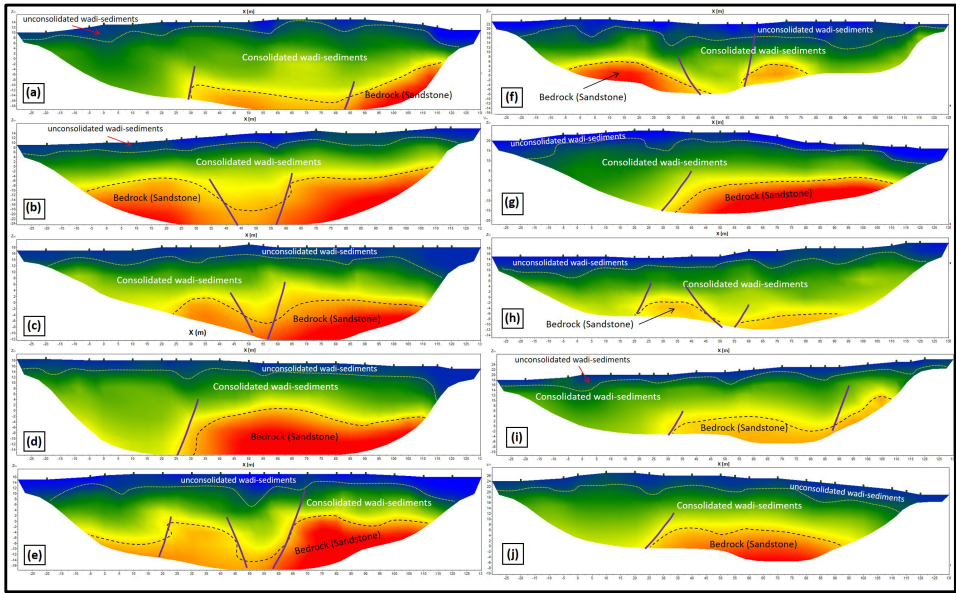


Fig. 8. Tomographic inversion results for profiles from SR-9 to SR-18 from (a) to (j), respectively. Black-dashed line indicates iso-velocity of 2300 m/s which represents top of non-rippable sandstone bedrock, and yellow-dotted line represents bottom boundary of Quaternary unconsolidated sandstone. Solid purple lines represent fault structure. Note: the colour scale for this figure is also the one in Figs. 6 and 7.

of normal faults (half grabens and domino-style normal faults), which are predicted and delineated by many authors, as highlighted in Section 1, by conducting Vertical Electrical Sounding (VES) surveys around the study area. For this reason, basement fracturing due to rifting structures, as well as normal faults, is the main reason for the basement topography variations. Profiles SR-1 to SR-18 (Figs. 6) exhibit faults with minor graben developed.

Suez well-3 in Fig. 9 indicates a sandstone section under the weathered layers of unconsolidated Wadi sediments. This sandstone incorporates calcareous cement that is occasionally argillaceous. It is worth mentioning that the deep resistivity curve reading is high (60 ohms), which is relatively higher than resistivity values from other wells near Suez well-3, which represents a perfect freshwater aquifer that starts at a depth of 12 metres. Also, the high neutron values indicate high porosity in this zone.

The interpreted well logs show high consistency with the SRT results, as follows: The first layer is composed of Quaternary Wadi sediments, followed by consolidated calcareous sandstone, and finally ended by the compacted argillaceous sandstone representing the bedrock.

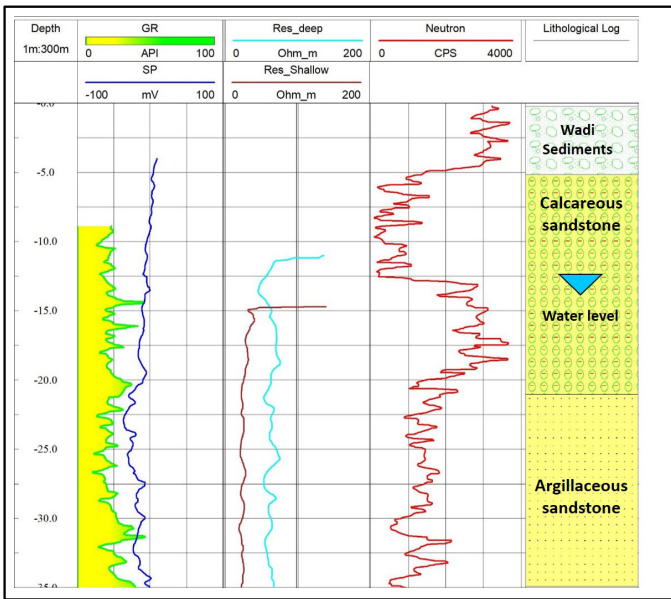


Fig. 9. Wireline dataset of the upper section of Suez well-3.

Pseudo 3D model generated in Fig. 10 was utilized to construct a three-dimensional model of the P-wave velocity distribution (Fig. 11) of the sub-surface to better visualize bedrock relief. Many low velocity zones were interpreted and were mainly due to normal fault structures (grabens), which have to be taken into consideration during the design and placement of foundation poles within the area under investigation.

## 5. Conclusion

This research aimed to examine the bedrock and outline its topography using seismic refraction data. A study was conducted at a proposed location for a crucial industrial facility in Egypt.

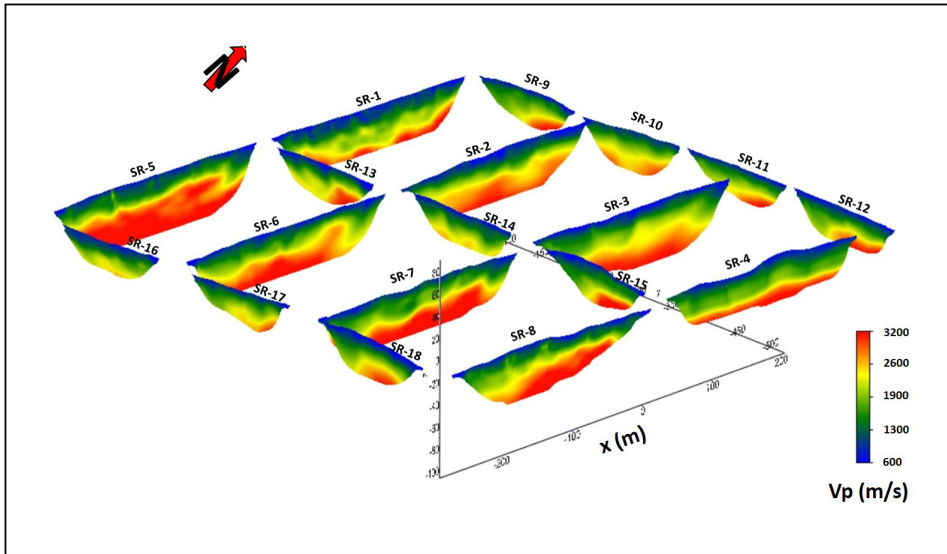


Fig. 10. Pseudo 3-D seismic refraction imaging representation of the eighteen spreads.

It was found that three geo-seismic layers are distinguished from the tomographic inversion results from top to bottom as follows: unconsolidated Wadi sediments with a relatively low-velocity range (400 m/s to 1100 m/s), and thickness between 0.5 m to 10 m, consolidated Wadi sediments with a velocity range (1200 m/s to 2000 m/s) with 8.5 m to 25 m in depth; and finally, sandstone bedrock of high velocity (2200 m/s to 3500 m/s), which correlates quite well with the electrical wireline logging results from a nearby borehole.

Imaging results revealed that the bedrock is intact to heavily fractured sandstone, reflecting the history of complex deformation in the Gulf of Suez region. Several faults trending NW–SE and NE–SW were detected, and bedrock topography variation is structurally controlled by normal faulting events due to the Red Sea rifting system.

At depths varying from 15 to 32 metres, the soil in the study area is believed to be compact to highly compact and appropriate for construction. The three-dimensional P-wave velocity model identified more competent areas for construction loads than others. The results of this research may be used for inexpensive and non-destructive geotechnical subsurface char-



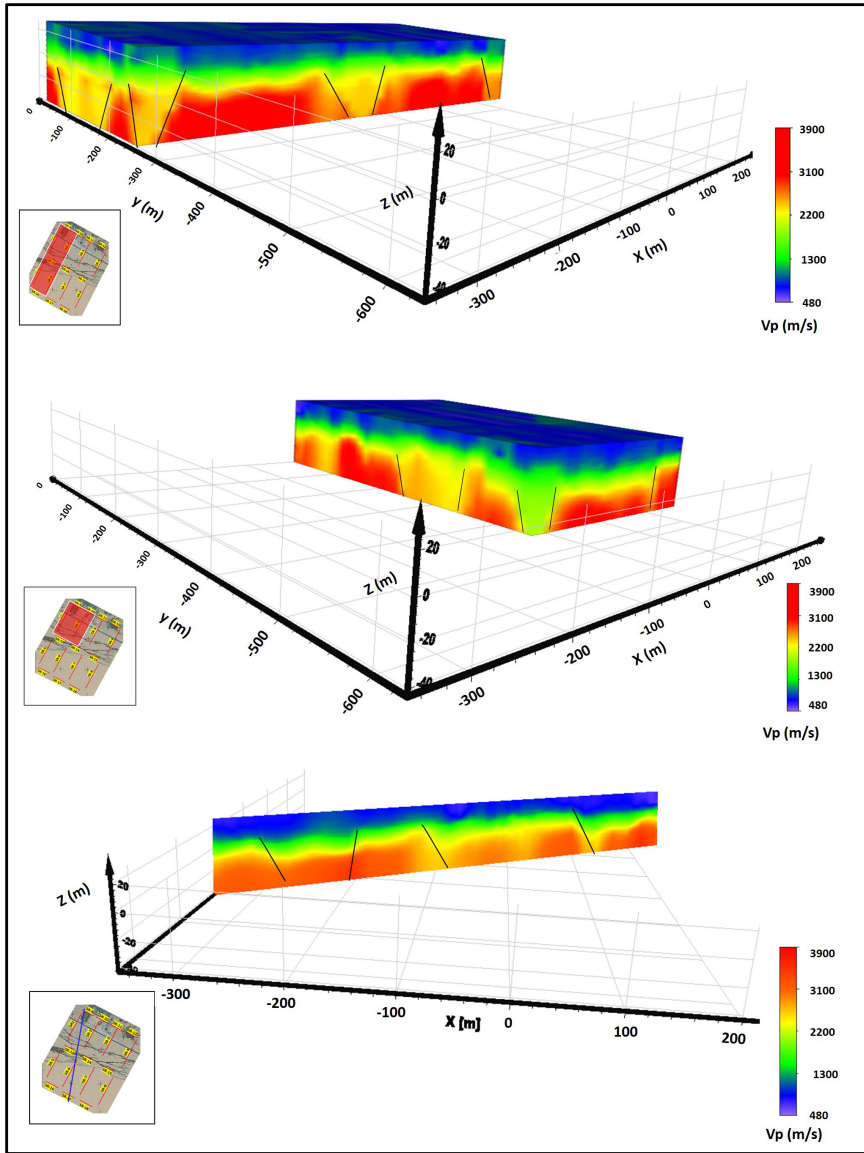


Fig. 11. Three-dimensional clipped planes generated from seismic refraction profiles grid to better visualize the lateral extent of the bedrock topography in the study area (top and middle), virtual direction slice generated from 3D model to better visualize faults affecting bedrock.

acterizations utilizing the seismic refraction technique, as well as for the preliminary design of the foundation poles and their depth.

**Acknowledgements.** Author would like to acknowledge the Nuclear Material Authority of Egypt for their support and for providing the access to the dataset.

**Data and materials are readily available.** Datasets created or analysed in the development of the current study are available from the corresponding author upon reasonable request.

**Code availability.** There is no code available in this work.

**Authors' contributions.** All authors contributed to the study conception and design. Material preparation, data collection and analysis were performed by the following authors: [Muhammad Ashraf El Hameedy], [Waleed Mohamed Mabrouk], [Ahmed Mohsen Metwally], and [Said Dahroug]. Data acquisition by [Mohamed Shokry Youssef]. The first draft of the manuscript was written by [Muhammad Ashraf El Hameedy] and all authors commented on previous versions of the manuscript. All authors read and approved the final manuscript.

**Declarations.** All authors certify that they have no affiliations with or involvement in any organization or entity with any financial interest or non-financial interest in the subject matter or materials discussed in this manuscript.

## References

- Abu El-Enain F. M., Ali M. M., Ismail A. S., 1997: Petrography, geochemistry and depositional history of the Eocene rocks in the area between northern Galala and Gabal Ataq, Western Gulf of Suez, Egypt. *Ann. Geol. Surv. Egypt*, **20**, 551–576.
- Akingboye A. S., Ogunyeye A. C., 2019: Insight into seismic refraction and electrical resistivity tomography techniques in subsurface investigations. *Rud.-Geolosko-Naft. Zb. (Min.-Geol.-Pet. Eng. Bull.)*, **34**, 1, 93–111, doi: 10.17794/rgn.2019.1.9.
- Araffa S. A. S., Abd El Nabi S. H., Helaly A. S., Dawoud M. A., Sharkawy M. S., Hassan N. M., 2022: Groundwater aquifer assessment using hydrogeophysical investigations: the case of western Al Ain Sokhna area, Gulf of Suez, Eastern Desert, Egypt. *Geocarto Int.*, **37**, 27, 16512–16533, doi: 10.1080/10106049.2022.2109762.
- Attwa M., Henaish A., 2018: Regional structural mapping using a combined geological and geophysical approach – A preliminary study at Cairo-Suez district, Egypt. *J. Afr. Earth Sci.*, **144**, 104–121, doi: 10.1016/j.jafrearsci.2018.04.010.
- Avseth P., Mavko G., Dvorkin J., Mukerji T., 2001: Rock physics and seismic properties of sands and shales as a function of burial depth. *SEG Technical Program Expanded Abstracts*, 1780–1783, doi: 10.1190/1.1816471.

- Azwin I. N., Saad R., Nordiana M., 2013: Applying the Seismic Refraction Tomography for Site Characterization. *APCBEE Procedia*, **5**, 227–231, doi: 10.1016/j.apcbee.2013.05.039.
- Bery A. A., 2013: High Resolution in Seismic Refraction Tomography for Environmental Study. *Int. J. Geosci.*, **4**, 4, 792–796, doi: 10.4236/ijg.2013.44073.
- Brixová B., Mosná A., Putiška R., 2018: Applications of shallow seismic refraction measurements in the Western Carpathians (Slovakia): case studies. *Contrib. Geophys. Geod.*, **48**, 1, 1–21, doi: 10.2478/congeo-2018-0001.
- Butchibabu B., Jha P. C., Sandeep N., Sivaram Y. V., 2023: Seismic refraction tomography using underwater and land based seismic data for evaluation of foundation of civil structures. *J. Appl. Geophys.*, **210**, 104934, doi: 10.1016/j.jappgeo.2023.104934.
- Butchibabu B., Khan P. K., Jha P. C., 2019a: Foundation evaluation of a repeater installation building using electrical resistivity tomography and seismic refraction tomography. *J. Environ. Eng. Geophys.*, **24**, 1, 27–38, doi: 10.2113/jeeeg24.1.27.
- Butchibabu B., Khan P. K., Jha P. C., 2019b: Foundation evaluation of underground metro rail station using geophysical and geotechnical investigations. *Eng. Geol.*, **248**, 140–154, doi: 10.1016/j.enggeo.2018.12.001.
- Caterpillar Inc., 2010: Caterpillar performance handbook (40th ed.): Caterpillar, Inc., Peoria, Ill., 1, 442 p.
- Conoco, 1987: Geological map of Egypt, Scale 1:500,000. NH36 SW-BENI SUEF sheet.
- El-Behiry M. G., Shedid A., Abu-Khadra A., El-Huseiny M., 2006: Integrated GIS and remote sensing for runoff hazard analysis in Ain Sukhna industrial area, Egypt. *J. King Abdulaziz Univ. Earth Sci.*, **17**, 1, 19–42, doi: 10.4197/ear.17-1.2.
- Hagedoorn J. G., 1959: The plus-minus method of interpreting seismic refraction sections. *Geophys. Prospect.*, **7**, 2, 158–182, doi: 10.1111/j.1365-2478.1959.tb01460.x.
- Han D., Nur A., Morgan D., 1986: Effects of porosity and clay content on wave velocities in sandstones. *Geophysics*, **51**, 11, 2093–2107, doi: 10.1190/1.1442062.
- Herlambang N., Riyanto A., 2021: Determination of bedrock depth in Universitas Indonesia using the seismic refraction method. *IOP Conf. Ser.: Earth Environ. Sci.*, **846**, 1, 012016, doi: 10.1088/1755-1315/846/1/012016.
- Hiltunen D. R., Cramer B. J., 2008: Application of seismic refraction tomography in karst terrane. *J. Geotech. Geoenviron. Eng.*, **134**, 7, 938–948, doi: 10.1061/(asce)1090-0241(2008)134:7(938).
- Jamiolkowski M., 2012: Role of geophysical testing in geotechnical site characterization. *Soils Rocks*, **35**, 2, 117–137, doi: 10.28927/SR.352117.
- Leucci G., Greco F., De Giorgi L., Mauceri R., 2007: Three-dimensional image of seismic refraction tomography and electrical resistivity tomography survey in the castle of Occhiola (Sicily, Italy). *J. Archaeol. Sci.*, **34**, 2, 233–242, doi: 10.1016/j.jas.2006.04.010.
- Mekkawi M. M., Abd-El-Nabi S. H., Farag K. S., Abd-Elhamid M. Y., 2022: Geothermal resources prospecting using magnetotelluric and magnetic methods at Al Ain



- AlSukhuna-Al Galala Albahariya area, Gulf of Suez, Egypt. *J. Afr. Earth Sci.*, **190**, 104522, doi: 10.1016/j.jafrearsci.2022.104522.
- Metwally A., Hanafy S., Guo B., Kosmicki M., 2017: Imaging of subsurface faults using refraction migration with fault flooding. *J. Appl. Geophys.*, **143**, 103–115, doi: 10.1016/j.jappgeo.2017.05.003.
- Moustafa A. R., Khalil S. M., 2020: Structural setting and tectonic evolution of the Gulf of Suez, NW Red Sea and Gulf of Aqaba Rift systems. In: Hamimi Z., El-Barkooky A., Martínez Frías J., Fritz H., Abd El-Rahman Y. (Eds.): *The Geology of Egypt. Regional Geology Reviews*. Springer, Cham, doi: 10.1007/978-3-030-15265-9\_8.
- Nurhandoko B. E. B., Matsuoka T., Watanabe T., Ashida Y., 1999: Land seismic refraction tomography using homogeneous velocity as initial model. *SEG Tech. Program Expand. Abstr.*, **18**, 1481–1484, doi: 10.1190/1.1820799.
- Othman A. A. A., Abdel Hafeez T. H., Youssef M. A. , Sabra M. E. M., 2015: Application of shallow seismic refraction survey to solve engineering problems, at Ain Al-Sokhna area, West Gulf of Suez, Egypt. *Ann. Geol. Surv. Egypt*, **XXXII**, 323–336, doi: 10.13140/RG.2.2.19839.30887.
- Oyedele K. F., Oladele S., Adedoyin O., 2011: Application of geophysical and geotechnical methods to site characterization for construction purposes at Ikoyi Lagos, Nigeria. *J. Earth Sci. Geotech. Eng.*, **1**, 1, 87–100.
- Ozcep F., Ozcep T., 2011: Geophysical analysis of the soils for civil (Geotechnical) engineering and urban planning purposes: Some case histories from Turkey. *Int. J. Phys. Sci.*, **6**, 5, 1169–1195, doi: 10.5897/ijps11.090.
- Palmer D., 1981: An Introduction to the generalized reciprocal method of seismic refraction interpretation. *Geophysics*, **46**, 11, 1508–1518, doi: 10.1190/1.1441157.
- Reynolds M. L., 1979: Geology of the Northern Gulf of Suez. *Ann. Geol. Surv. Egypt*, **IX**, 322–343.
- Reynolds J. M., 1997: An introduction to applied and environmental geophysics. John Wiley & Sons, Inc., New York, USA, 796 p.
- Salem A. S., 1988: Geological and hydrogeological studies on the area between Gebel Ataqa and Northern Galala plateau, Egypt. Ph.D. thesis, Fac. Sci., Geol. Dept., Zagazig Univ., Egypt, 271 p.
- Schlindwein V., Bönnemann C., Reichert C., Grevemeyer I., Flueh E., 2003: Three-dimensional seismic refraction tomography of the crustal structure at the ION site on the Ninetyeast Ridge, Indian Ocean. *Geophys. J. Int.*, **152**, 1, 171–184, doi: 10.1046/j.1365-246x.2003.01838.x.
- Sheehan J. R., Doll W. E., Mandell W. A., 2005: An evaluation of methods and available software for seismic refraction tomography analysis. *J. Environ. Eng. Geophys.*, **10**, 1, 21–34, doi: 10.2113/jeeg10.1.21.
- Sheriff R. E., Geldart L. P., 1995: *Exploration Seismology*, 2nd ed. Cambridge University Press, New York, USA, 628 p.
- Sultan A. S., Essa K. S. A. T., Khalil M. H., El-Nahry A. E. H., Galal A. N. H., 2017: Evaluation of groundwater potentiality survey in south Ataqa-northwestern part of Gulf of Suez by using resistivity data and site-selection modeling. *NRIAG J. Astron. Geophys.*, **6**, 1, 230–243, doi: 10.1016/j.nrjag.2017.02.002.

- Thurber C. H., Ritsema J., 2007: Theory and Observations – Seismic Tomography and Inverse Methods (1.10). In: Schubert G. (Ed.): *Treatise on Geophysics*, Elsevier EBooks, 323–360, doi: 10.1016/b978-044452748-6.00009-2.
- White D. J., 1989: Two-dimensional seismic refraction tomography. *Geophys. J. Int.*, **97**, 2, 223–245, doi: 10.1111/j.1365-246x.1989.tb00498.x.
- Whiteley J. S., Chambers J. E., Uhlemann S., Boyd J., Cimpoiasu M. O., Holmes J. L., Inauen C. M., Watlet A., Hawley-Sibbett L. R., Sujitapan C., Swift R. T., Kendall J. M., 2020: Landslide monitoring using seismic refraction tomography – The importance of incorporating topographic variations. *Eng. Geol.*, **268**, 105525, doi: 10.1016/j.enggeo.2020.105525.
- Younis A., Osman O. M., Khalil A. E., Nawawi M. G. M., Soliman M. F., Tarabees E. A., 2019: Assessment groundwater occurrences using VES/TEM techniques at North Galala plateau, NW Gulf of Suez, Egypt. *J. Afr. Earth Sci.*, **160**, 103613, doi: 10.1016/j.jafrearsci.2019.103613.
- Youssef M. A. S., 2020: Geoelectrical analysis for evaluating the aquifer hydraulic characteristics in Ain El-Soukhna area, West Gulf of Suez, Egypt. *NRIAG J. Astron. Geophys.*, **9**, 1, 85–98, doi: 10.1080/20909977.2020.1713583.
- Youssef M. I., Abdel Rahman M. A., 1978: Structural map sensing of the area between Gabal Ataqa and northern Galala plateau, Gulf of Suez region, Egypt. *10th Arab Petroleum Conf., Tripoli, Libya*, 135(C-3), 8 p.